AIAA JOURNAL
Vol. 44, No. 6, June 2006

Analysis of Inflated Conical Cantilever Beams in Bending

Sebastiaan L. Veldman* and Otto K. Bergsma†
Technical University of Delft, 2600 GB Delft, The Netherlands

The bending behavior of straight inflated beams has been studied for several decades. A number of theoretical models exist that predict the load deflection behavior of the beams in bending. The various models approach the problem in different ways. This is especially the case by the way the wrinkling and collapse load are defined. A definition for the collapse load for straight cylindrical beams has been modified to suit single- and double-curved beams. The definition for the collapse load is used to derive a load deflection model for truncated conical beams. The effect of a beam being conical instead of straight is of extra significance for an inflated beam because it changes the prestress distribution introduced by the internal overpressure. Increasing the prestresses will result in an increased wrinkling and collapse load. The primary objective is to derive a load deflection model for inflated truncated conical beams. A secondary goal is to optimize the geometry to minimize the deflection using the same amount of skin material. The optimized geometry and the straight cylindrical beam made of polyphenylenesulphide foil will be analyzed and compared using finite element analysis.

Nomenclature

C	=	constant
E	=	modulus of elasticity
L	=	length
M	=	moment
p	=	overpressure
Q	=	force
r	=	radius
s	=	coordinate in meridional direction
t	=	thickness
W	=	weight
x, y, z	=	Cartesian coordinates
α	=	semivertex angle
γ	=	shear strain; correlation factor
ε	=	strain
θ	=	coordinate in parallel direction
κ	=	curvature parameter
ν	=	Poisson ratio
ρ	=	density
σ	=	stress
τ	=	shear stress

Subscripts

coll	=	collapse
cyl	=	cylinder
max	=	maximum
min	=	minimum
w	=	wrinkling initiation

I. Introduction

THE use of truncated conical beams instead of straight beams can improve the efficiency of the beam and allow for a conical deployment system.[1] Relatively little literature was found on the bending of pressurized truncated cones. General design criteria for buckling of thin-walled truncated cones are given by Weingarten et al.[2] They provide a conservative expression for the collapse moment of a pressurized conical shell under pure bending. Their expression relies on data that need to be acquired from a figure. Seide[3] provides another expression for the collapse of a conical shell in bending. He states that the critical stress for a conical shell under axial compression should be equal to the critical stress of a cylinder having the same local radius of curvature. This is a similar approach to relating the buckling load of axially compressed cylinders to that of truncated cones.[3–9] Arbocz[10] confirmed that such an approach is valid for cones with a semivertex angle smaller than 45 deg. The cones under review in this paper all have an angle smaller than 10 deg.

On an inflated cantilever beam subjected to a transverse shear load, the location where wrinkles will be initiated is dependent on the taper ratio. This is the ratio between minimum and maximum radius. Bending experiments[11] have demonstrated that for small enough taper ratios wrinkles will be initiated at a location on the beam away from the clamped end.[12] At a straight cylindrical beam in the same load case, wrinkles will always first be formed at the clamped end. This is an important effect to take into consideration because when the location of wrinkling initiation is not at the clamped end the load at which wrinkles are initiated reduces.

The objective of this paper is to understand the influence of geometry on the load deflection of an inflated beam made of an isotropic material and to find an optimized geometry. This optimized geometry is found by minimizing the deflection using the same amount of polyphenylenesulfide (PPS) foil material.

The structure of the paper is as follows. First a theoretical bending model for axial symmetrical beams having a circular cross section will be discussed. The theory will be applied in the third section to optimize the geometry. Subsequently, the bending behavior of the optimized beams will be compared to finite element analysis results. A brief conclusion is given at the end of the paper.

II. Theoretical Bending Model of Truncated Inflated Beams

Figure 1 shows a beam that is simply supported at the yz plane and loaded at the end cap. An orthogonal grid can be defined on the surface. This grid consists of meridian and parallel curves, which are lines on the surface for which parameters θ and s, respectively, are constant. Both lines are lines of principal curvature on the surface.[13]

The radius is expressed as

$$r = [1 + (\mathrm{TR} - 1)(x/L)]r_{\max} \tag{1}$$

$$r_\alpha = r/\cos\alpha \tag{2}$$

Received 1 March 2005; presented as Paper 2005-1805 at the 46th Structures, Structural Dynamics, and Materials Conference (6th Annual Gossamer Spacecraft Forum), Austin, TX, 18–21 April 2005; revision received 8 October 2005; accepted for publication 27 October 2005.

*Associate Researcher, P.O. Box 5058, Faculty of Aerospace Engineering. Member AIAA.

†Associate Professor, P.O. Box 5058, Faculty of Aerospace Engineering.

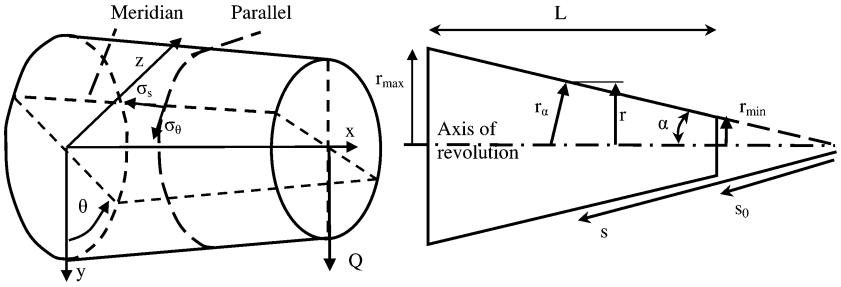

Fig. 1 Parameter definitions.

and the taper ratio (TR) is defined as

$$\mathrm{TR} = r_{\min}/r_{\max} \tag{3a}$$

The semivertex angle α follows from

$$\cos\alpha = \frac{L}{\sqrt{L^2 + (1-\mathrm{TR})^2 r_{\max}^2}} \tag{3b}$$

When a membrane approach is used and it is assumed that the deflections are small, the stresses due to pressurization and shear load Q in the directions of the two principal curves can be written as

$$\sigma_s = (pr_\alpha/2t) - \left(Q\cos\theta \Big/ \pi t r_\alpha^2\right)(L-x) \tag{4a}$$

$$\sigma_\theta = pr_\alpha/t \tag{4b}$$

$$\tau_{s\theta} = -\left(Q\sin\theta \Big/ \pi t r_\alpha^2\right)(L-x) \tag{4c}$$

A full derivation of Eqs. (4a–4c) is given by Veldman.[14] The stress strain relations are

$$\varepsilon_s = (\sigma_s/E) - (\nu\sigma_\theta/E) \tag{5a}$$

$$\varepsilon_\theta = (\sigma_\theta/E) - (\nu\sigma_s/E) \tag{5b}$$

$$\gamma_{s\theta} = (\tau_{s\theta}/G_{x\theta}) \tag{5c}$$

Substitution of Eqs. (2), (4a), and (4b) into Eq. (5a) gives

$$\varepsilon_s = (pr_\alpha/2tE)(1-2\nu) - \left(Q\cos\theta \Big/ \pi t E r_\alpha^2\right)(L-x) \tag{6}$$

When the material of the beam is fully taut, the beam will behave like an Euler–Bernoulli beam. The expression for curvature is given by

$$\kappa = (\sigma_{s\cdot\max} - \sigma_{s\cdot\min})/2Er_\alpha \tag{7}$$

The maximum and minimum stresses in the s direction occur at $\theta = \pi$ and $\theta = 0$, respectively. Substitution of Eqs. (2) and (4a) into Eq. (7) gives

$$\kappa = \left(Q \Big/ \pi t E r_\alpha^3\right)(L-x) \tag{8}$$

Substitution of Eq. (8) into Eq. (6) yields

$$\varepsilon_s = (pr_\alpha/2tE)(1-2\nu) - r_\alpha\cos\theta\kappa \tag{9}$$

In a partly wrinkled cross section, the stress and strain distribution will be different from a fully taut cross section. For the taut section of a partly wrinkled cross section, a strain distribution in the s direction is proposed that is comparable to one proposed for straight cylindrical inflated beams,[15]

$$\varepsilon_s = C_1 - r_\alpha\cos\theta\kappa \tag{10}$$

Substitution in Eq. (5a) and rewriting gives

$$\sigma_s = E(C_1 - r_\alpha\cos\theta\kappa) + \nu\sigma_\theta \tag{11}$$

Replacing the angle θ with the wrinkling angle θ_w allows for solving Eq. (11) for C_1,

$$C_1 = -\nu(\sigma_\theta/E) + r_\alpha\cos\theta_w\kappa \tag{12}$$

Wrinkles will essentially be modeled using a modified Poisson's ratio (see Ref. 15), which can be found by substitution of ν by the modified Poisson's ratio λ. Substitution in Eq. (11) of Eq. (12) gives the stress distribution in the s direction in the taut region of the partly wrinkled cross section:

$$\sigma_s = r_\alpha E\kappa(\cos\theta_w - \cos\theta) \tag{13}$$

Balance of forces and moments yields

$$p\pi r_\alpha^2 = 2t\int_{\theta_w}^{\pi} \sigma_s r_\alpha \,\mathrm{d}\theta \tag{14a}$$

$$Q(L-x) = -2t\int_{\theta_w}^{\pi} \sigma_s r_\alpha^2\cos\theta \,\mathrm{d}\theta \tag{14b}$$

Solving Eqs. (14a) and (14b) and dividing Eq. (14b) by Eq. (14a) yields an expression with which the wrinkling angle can be obtained:

$$\frac{Q(L-x)}{\pi p r_\alpha^3} = \frac{1}{2}\frac{(\cos\theta_w\sin\theta_w + \pi - \theta_w)}{((\pi-\theta_w)\cos\theta_w + \sin\theta_w)} \tag{15}$$

Equation (15) is valid in the case in which the material is modeled as a true membrane. However, as shown by Veldman et al.,[12] thin foils cannot automatically be modeled as a true membrane but may need to be modeled as a shell. It was shown that PPS foil should be treated as a shell not as a membrane. To treat it as a shell, the collapse moment needs to be studied. Weingarten et al.[2] predict the collapse of a pressurized truncated cone under pure bending using the following expression:

$$M_{\mathrm{coll}} = \left\{\left[\gamma \Big/ \sqrt{3(1-\nu^2)}\right] + \Delta\gamma\right\}\pi E r_{\min}(t\cos\alpha)^2 + \left(p\pi r_{\min}^3 \Big/ 2\right) \tag{16}$$

The parameter γ is a correlation factor to account for the difference of the classical theory and predicted instability loads and a value of 0.41 is recommended. The parameter $\Delta\gamma$ is an increase in buckling correlation factor due to pressure. This parameter is acquired from a plot. Besides that this procedure is somewhat inaccurate, Eq. (16) provides a relative conservative prediction because the minimum radius is used. In the literature[3–10] on the collapse of truncated cones in axial compression, a collapse criterion is used that follows from collapse analysis of straight cylindrical cones having an equal radius as the local radius r_α of the conical shell. Furthermore, it is also stated that the critical stress for an straight cylindrical beam in bending is equal to the critical stress of a straight cylindrical beam in axial compression.[11] Based on these findings, it is assumed that the critical stress for a pressurized truncated conical beam is equal to that of a straight cylinder having the same local radius and thickness.

A semiempirical expression for the collapse load for straight pressurized beams has been derived by Veldman et al.[12] The collapse

moment for a pressurized truncated cone made of isotropic material becomes

$$M_{\text{coll}} = (\pi/4)\pi p r_\alpha^3 + \left(2\sqrt{2}/9\right)\pi E r_\alpha t^2 \times \sqrt{[1/(1-\nu^2)] + 4(p/E)(r_\alpha/t)^2} \tag{17}$$

On examination of Eq. (15) it follows that collapse takes place when the wrinkling angle θ_w approaches π. The true membrane solution[16] for the collapse moment is equal to the first part of Eq. (17) without the correction factor $\pi/4$. To make Eq. (15) suitable for shells, it needs to be combined with Eq. (17). It is proposed that wrinkling takes place as soon as the sum of the theoretical buckling collapse load of shells [second part of right-hand side of Eq. (17)] and the membrane wrinkling load are reached. Hence, Eq. (17) becomes

$$Q(L-x) = \frac{(\cos\theta_w \sin\theta_w + \pi - \theta_w)}{[(\pi - \theta_w)\cos\theta_w + \sin\theta_w]} \frac{\pi}{8} \pi p r_\alpha^3 + \frac{2\sqrt{2}}{9} \pi E r_\alpha t^2 \sqrt{\frac{1}{1-\nu^2} + 4\frac{p}{E}\left(\frac{r_\alpha}{t}\right)^2} \tag{18}$$

Equation (18) is used to determine the wrinkling angle. Solving Eq. (14b) yields the following expression for curvature in the partly wrinkled cross section:

$$\kappa = \frac{Q(L-x)}{\pi t r_\alpha^3 E(\cos\theta_w \sin\theta_w + \pi - \theta_w)} \tag{19}$$

Equation (8) is the curvature expression for the taut cross sections. For small deflections, the deflection can be found solving the following differential equation:

$$\frac{\mathrm{d}^2 y}{\mathrm{d}x^2} = \kappa \tag{20}$$

III. Geometrical Optimization for Minimum Deflection

A commonly known optimization criterion is to design for minimum deflection while keeping the applied loads and weight constant. The optimization problem is accompanied by one equality constraint and two inequality constraints. The following expressions describe the entire problem:

$$\text{Minimum (deflection)} \tag{21}$$

$$W_{\text{cone}} = W_{\text{cyl}} \tag{22a}$$

$$\sigma_1 - \sigma_{\max} \geq 0 \tag{22b}$$

$$Q_w - Q \geq 0 \tag{22c}$$

The subscripts 1 and 2 denote the first and second in-plane principal stresses. The last constraint equation (22c) implies that the wrinkling load should be larger than or equal to the applied load. Should this constraint not be satisfied, then it becomes very difficult to verify analytically whether the second constraint equation (22b) will be valid. The theory presented in the preceding section uses a modified Poisson's ratio to model the deformation behavior in a global manner such as a load deflection curve. For local behavior, such as stress levels, the theory in a postwrinkled situation should not be relied on. The optimization variables are the maximum radius, the TR, and the skin thickness of PPS foil. Both end caps of the beams will be made of 1-cm-thick polystyrene foam. For comparison the maximum allowable stress is set equal to the maximum in-plane stress occurring in a straight cylindrical beam in bending. The weights of the cylinder and a truncated cone are found using the following equations:

$$W_{\text{cyl}} = \rho_{\text{cap}} 2\pi r^2 t_{\text{cap}} + \rho_{\text{pps}} 2\pi r t L \tag{23}$$

$$W_{\text{cone}} = \rho_{\text{cap}} \pi t_{\text{cap}} r_{\max}^2 (1 + \text{TR}^2) + \rho_{\text{pps}} \pi t r_{\max} (1 + \text{TR}) \times \sqrt{r_{\max}^2 (\text{TR} - 1)^2 + L^2} \tag{24}$$

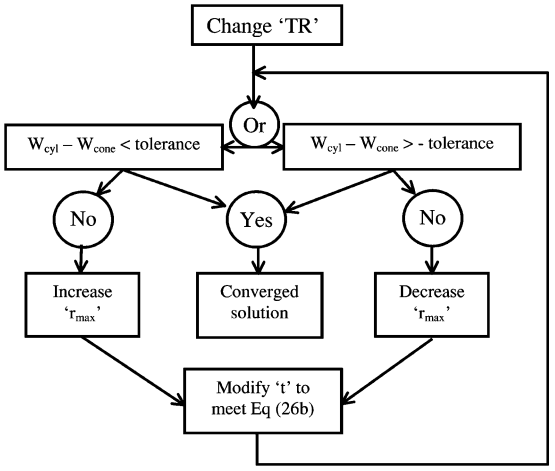

Fig. 2 Optimization scheme.

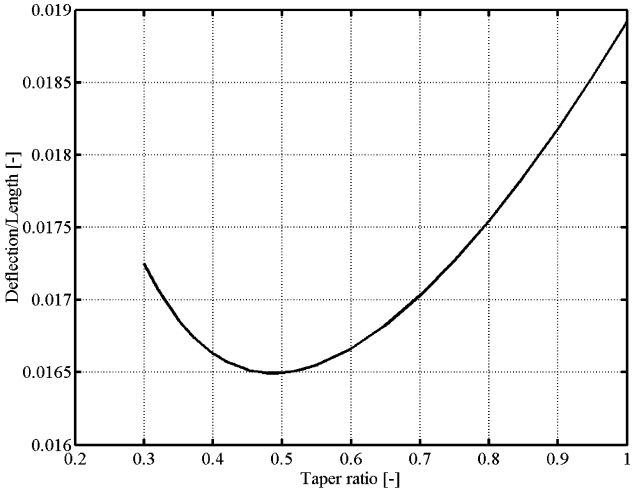

Fig. 3 Relation between TR and deflection for beams with same weight; applied tip load 3.7 N and beam length 1 m.

The flowchart in Fig. 2 shows the way the optimization has been performed. The first step is to have a specific TR. Then a check is made whether the new geometry results in a lower or heavier weight than the cylindrical beam. Should the weight difference be within the set tolerance, than the solution is considered to be converged. When the solution is not converged, the maximum radius is either increased or decreased depending on whether the weight difference is positive or negative, respectively. The next step is to adjust the skin thickness to meet the maximum allowable stress constraint equation (22b). After this adjustment, the loop goes back to the start, and again the weight of the cone is compared to the cylinder weight.

After convergence is achieved, a check is done for the no-wrinkling constraint equation (22c). For each new geometry, the deflection at the specified applied load is found. Figure 3 shows the deflection relative to the TR. It is shown that a minimum deflection can be found for a TR close to 0.5 for a 1-m-long beam. The TR slightly increases when the length increases, and the optimum TR is by no means valid for every length or material.

It was found that as the length of the beams increases the difference in deflection of a beam having an optimum TR and a cylindrical beam becomes smaller. For 1-m-long beams, the minimum of the curve of Fig. 3 is 87% of the maximum, whereas for 20-m-long beams, this is 92%. The most optimum 1-m-long beam has a maximum radius of 5.68 cm, a TR of 0.5, and a skin thickness of 0.0703 mm.

IV. Comparison of Finite Element Analysis of a Straight and Conical Beam

This section deals with the finite element analysis of inflated beams using the finite element package ABAQUS. Both a straight beam and a beam with a TR of 0.5, that is, the optimum geometry derived in the preceding section, will be analyzed and compared. The most elaborate analysis was performed on the straight beam, and the results were compared to experimental results and the results of the theoretical model derived by Veldman et al.[12]

A. Finite Element Analysis of Straight Cylindrical Beam

The finite element model consists of two parts, a circular cylindrical beam and an end cap. The 1-m-long, 0.05-m radius beam is made of 0.06-mm-thick PPS foil, which has a Young's modulus of 2.85 GPa and a Poisson's ratio of 0.35. The end cap is made of 5-mm-thick aluminum, which has a Young's modulus of 70 GPa and a Poisson's ratio of 0.3. The end cap was connected to the beam using pin multiple point constraints. This constraint type enforces the nodes of the slave element to have the same displacements as the corresponding nodes of the master element. The end cap was selected as master surface. Encastre boundary conditions were applied to the other end of the beam to model the clamped side of the beam. The mesh density can significantly influence the results, especially when buckling occurs. However, in general, the finer the mesh the more computational time it costs. Therefore, the aim is to have the coarsest mesh that still results in an accurate enough solution. The mesh does not have to be fine everywhere as long as it is fine in the area where wrinkles occur. A biased seed will, therefore, be used over the length of the beam, and the smallest element length will be at the supported end. This is where wrinkles will be formed first because the applied moment is the largest. The elements used were S4 general purpose, finite-membrane-strain shell elements.[17] A convergence analysis on buckling or wrinkling load was performed to find the appropriate mesh. This wrinkling load follows from the multiplication of the lowest eigenvalue and the perturbation load added with the pre load. The eigenvalues were obtained after a pressure of 0.2 bar was applied to the beam. A structured mesh was applied to the beam. This type of meshing allows for tailoring the mesh density in two directions. In this case, the number of elements around the circumference and along the length of the beam can be varied to investigate the influence of the mesh to the results. Table 1 shows the results of the convergence analysis. Around the circumference all elements were evenly distributed.

The applied mesh, however, is not one of the meshes listed in Table 1. When Table 1 is examined, it can be observed that increasing the number of elements in the length direction has a larger effect on the wrinkling load than increasing the number of elements in the circumferential direction. Furthermore, the difference in wrinkling loads between 240 and 320 elements in length direction is limited. The applied mesh has only 200 elements along the length of the beam, but the bias ratio is 5 instead of 2. It predicts a wrinkling load of 5.457 N, whereas the wrinkling load predicted by the analytical theory is 5.385 N. Around the circumference the elements are not evenly distributed anymore. The circumference is divided in four equally sized regions. The borders are formed by the xy plane and the xz plane. Figure 1 shows the coordinate system. Instead of a tapered beam, a straight beam is used. The two regions that have a positive y coordinate have a biased seed as well to have the aspect ratio of the elements as close to 1 as possible. Each of the two regions has 18 seeds and a bias ratio of 1.5 that is directed to the y axis (Fig. 1). The two regions that have a negative y coordinate are equipped with 14 evenly distributed elements. The advantage of this mesh over the other meshes analyzed is that does not have as many elements as the finest mesh and that the aspect ratio of the elements that will be in the wrinkled region is smaller than those of the finest meshes. The largest aspect ratio of an element of the mesh having 320 elements in length direction and 72 around the circumference is 3.63. The element involved is located at the supported end. During the analysis, it turned out that at some stage in the analysis the very fine mesh failed to converge and as a result the analysis aborted. Figure 4 shows the results of the finite element analysis of a straight inflated beam loaded by a shear load. Three curves are shown in Fig. 4. The dashed curve represents the result of the finite element analysis; the circle markers are experimentally obtained results; and the dash–dot curve is the prediction of the analytical theory. First observe from these results that all three curves correspond very well for the linear part. The nonlinear part, however, exhibits some differences between the two analysis methods and the experimental result. The analytical theory is an underprediction, and the finite element analysis is an overprediction compared to the experimental results. The finite element results, however, are closer to the experimental result[12] than the analytical theory ones. Although the finite element analysis overpredicts the strength of the

Table 1 Wrinkling loads related to different meshes

Elements in circumferential direction	Elements in length direction[a]			
	80	160	240	320
40	9.31	6.18	5.59	5.38
56	9.18	6.14	5.56	5.36
72	9.12	6.12	5.55	5.35

[a]Over the length, a bias ratio of 2 was applied; that is, node distance on one side is two times larger than on the opposite side.

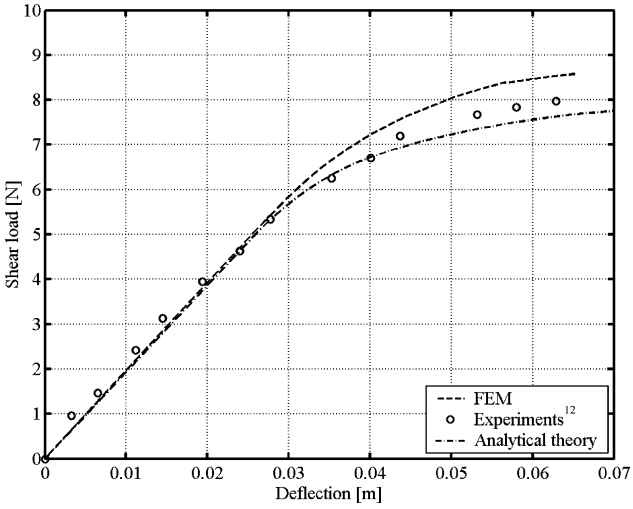

Fig. 4 Comparison between results of experiments,[12] finite element analysis, and analytical theory of straight beam of PPS foil at 0.2-bar pressure.

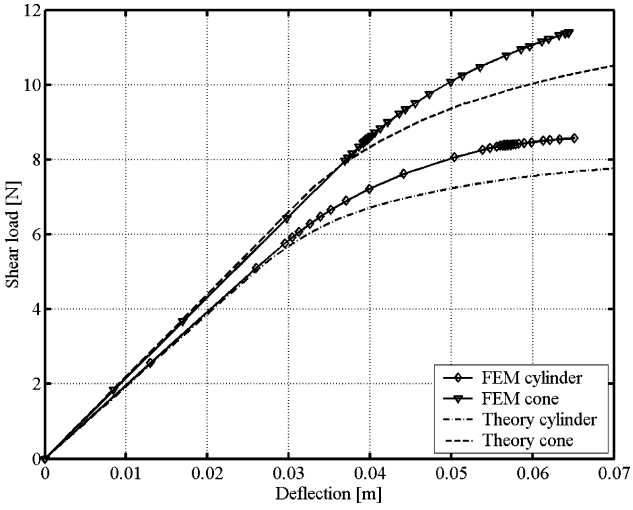

Fig. 5 Comparison between load deflection curve of cone (TR = 0.5, r_{max} = 5.68 cm, and t = 0.0703 mm) and straight beam r = 5 cm and t = 0.06 mm: finite element analysis and analytical theory results.

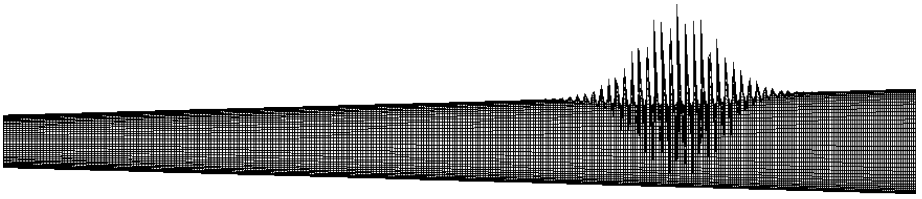

Fig. 6 Shape of first eigenmode of optimized truncated cone; deformation scale factor = 102.7.

inflated beam, it demonstrated that a problem like this can fairly successfully be analyzed using finite elements.

B. Finite Element Analysis of Conical Beam

The geometry of the conical beam has been derived in the preceding section. The truncated cone has a maximum radius of 5.68 cm at the supported end, a minimum radius of 2.84 cm, and a skin thickness of 0.0703 mm. Similar to the straight beam, the skin material is made of PPS foil and the end cap is made of aluminum. No significant mesh convergence study was performed for the conical beam. Instead, a similar mesh to that of the straight beam was applied to this type of beam. The bias ratio in the length direction, however, was 3 instead of 5 because, otherwise, the aspect ratio of the elements near the smallest radius would become too large. Figure 5 shows a comparison between load deflection behavior of the conical beam and the straight beam. Both results of the finite element and theoretical analysis are given. As Fig. 5 shows, the difference in the nonlinear part of the curves between the theory and the finite element results is similar for the cone and for the cylinder. It also shows that, as predicted by the analytical theory, the conical beam has a larger bending stiffness than the cylindrical beam. The wrinkling load predicted by the analytical theory is 7.61 N, whereas the one predicted by the finite element analysis is 7.05 N.

Figure 6 shows the shape of the first eigenmode of the truncated cone subjected to a shear load. A close examination of the buckling mode shape showed that the number of elements per half-wavelength is close to five. It can be observed that wrinkles are no longer initiated at the supported end but at some distance away from the end. This phenomenon is also predicted by the analytical theory. Experiments described by Veldman[11] have shown this effect happening in a nylon foil tapered beam having a taper ratio of 0.5 as well.

V. Conclusions

An analysis of the load deflection behavior of inflated conical beams made of isotropic material is presented. An analytical model used for straight cylindrical beams has been modified to suit conical beams. The purpose of this paper was to demonstrate the influence of geometry on the load deflection behavior of inflated beams. To illustrate this influence, the geometry of a conical beam has been optimized for minimum deflection at the same load and with the same amount of material. This optimization resulted in a TR of 0.5, an increased maximum radius of 5.68, and an increased thickness of 0.0703 mm. A finite element analysis was performed for comparison. First, a straight beam having a radius of 0.05 m and made of PPS foil was analyzed. A modal analysis was performed to find a prediction for the wrinkling load and to find an appropriate mesh. It was found that a mesh having the finest distribution at the location where wrinkles will occur was best in terms of computational time and wrinkling load accuracy. The predicted wrinkling load obtained with the modal analysis is only 1.3% larger than the analytical prediction. For the linear part, there was very good correlation to both the theoretical model and to the experimental results. For the nonlinear part of the load deflection curve, the finite element model provided an overestimation in the sense that the residual bending stiffness is larger at a given shear load compared to both theory and experiments. Just like the straight beam, the finite element results of the optimized conical beam correlate very well with the theory for the linear part. The nonlinear part, like the straight beam, shows that the finite element prediction has more residual stiffness than the analytical theory.

Acknowledgment

The authors thank J.M.A.M. Hol for his advice on finite element modeling.

References

[1]Lichodziejewski, D., Cravey, R., and Hopkins, G. "Inflatably Deployed Membrane Waveguide Array Antenna for Space," AIAA Paper 2003-1649, 2003.

[2]Weingarten, V. I., and Seide, P., "Buckling of Thin-Walled Truncated Cones," NASA SP-8019, Sept. 1968.

[3]Seide, P., "A Donnell Type Theory for Asymmetrical Bending and Buckling of Thin Conical Shells," *Journal Applied Mechanics*, Vol. 24, No. 4, 1957, pp. 547–552.

[4]Esslinger, M., and Geier, B., "Buckling and Post-Buckling Behaviour of Conical Shells Subjected to Axisymmetric Loading and of Cylinders Subjected to Bending," *Theory of Shells*, edited by W. T. Koiter and G. K. Mikhailov, North-Holland, Amsterdam, 1980, Chap. 2.

[5]Hausrath, A. H., and Dittoe, F. A., "Development of Design Strength Levels for the Elastic Stability of Monocoque Cones Under Axial Compression," *Collected Papers on Instability of Shell Structures*, NASA TN-D 1510, 1962, pp. 45–56.

[6]Seide, P., "A Survey of Buckling Theory and Experiment for Circular Conical Shells of Constant Thickness," *Collected Papers on Instability of Shell Structures*, NASA TN-D-1510, 1962, pp. 401–426.

[7]Spagnoli, A., and Chrissanthopoulos, M. K., "Buckling Design of Stringer-Stiffened Conical Shells in Compression," *Journal of Structural Engineering*, Vol. 125, No. 1, 1999, pp. 40–48.

[8]Zhang, G. Q., "Derivation of the Governing Equations of Anisotropic Conical Shells," Faculty of Aerospace Engineering, Rept. LR-609, Delft Univ. of Technology, Delft, The Netherlands, Jan. 1989.

[9]Zhang, G. Q., "Stability Analysis of Anisotropic Conical Shells," Ph.D. Dissertation, Faculty of Aerospace Engineering, Delft Univ. of Technology, Delft Univ. Press, Delft, The Netherlands, June 1993.

[10]Arbocz, J., "Buckling of Conical Shells Under Axial Compression" NASA CR 1162, Jan. 1968.

[11]Veldman, S. L., "Load Analysis of Inflatable Truncated Cones," AIAA Paper 2003-1827, 2003.

[12]Veldman, S. L., Bergsma, O. K., Beukers, A., and Drechsler, K., "Load Deflection Behavior of Inflated Beams Made of Various Foil Materials," AIAA Paper 2004-1504, 2004.

[13]Brush, D. O., and Almroth, B. O., *Buckling of Bars, Plates, and Shells*, McGraw–Hill, New York, 1975, Chap. 6.

[14]Veldman, S. L., "Design and Analysis Methodologies for Inflated Beams," Ph.D. Dissertation, Faculty of Aerospace Engineering, Delft Univ. of Technology, Delft Univ. Press, Delft, The Netherlands, June 2005.

[15]Stein, M., and Hedgepeth, J. M., "Analysis of Partly Wrinkled Membranes," NASA TND 813, June 1961.

[16]Comer, R. L., and Levy, S., "Deflections of an Inflated Circular-Cylindrical Cantilever Beam," *AIAA Journal*, Vol. 1, No. 7, 1963, pp. 1652–1655.

[17]"ABAQUS Theory and Standard Users Manual," Ver. 6.3-3, Hibbit, Karlsson and Sorensen, Inc., Providence, RI, 2003.

M. Ahmadian
Associate Editor